JOURNAL OF MATERIALS SCIENCE 20 (1985) 355–367

Matrix solidification and the resulting residual thermal stresses in composites

JOHN A. NAIRN, PAUL ZOLLER
Central Research and Development Department, E. I. Du Pont de Nemours and Company, Du Pont Experimental Station, Wilmington, Delaware 19898, USA

The disparate thermal expansion properties of the fibres and matrices in high-performance composites lead to an inevitable build up of residual thermal stresses during fabrication. We first discuss the thermal expansion behaviour of thermoplastic and thermoset polymers that may be used as high-performance composite matrices. The three classes of polymers considered are epoxies, amorphous thermoplastics, and semi-crystalline thermoplastics. The relevant thermal expansion data for prediction of the magnitude of the residual stresses in composites is the zero (atmospheric)-pressure thermal expansion data; these data are plotted for a range of thermoplastics and a typical epoxy. Using the technique of photoelasticity, we have measured the magnitude of the residual stresses in unidirectional graphite composites with an amorphous thermoplastic matrix (polysulfone) and with an epoxy matrix (BP907). The temperature dependence of the residual stress build up and the resulting magnitude of the residual stresses correlate well with the thermal and physical properties of the matrix resin.

1. Introduction

By design, composites are made of constituents with very different mechanical properties. The properties of the main constituents, matrix and fibres, can differ widely. One of these properties is the thermal expansion behaviour. Thermal expansion behaviour is important because processing of composites almost always takes place at temperatures 150 to 300° C above ambient. Over this temperature range, there are very sizeable volume changes in typical matrix resins, and generally smaller volume changes in fibres. In addition, the dimensional changes of the fibres commonly used in advanced composites, such as Kevlar aramid fibres, or graphite, are highly anisotropic and they are often put down in anisotropic arrays. As a consequence, one can expect both anisotropic dimensional changes and the development of anisotropic states of thermal stress in composites.

The temperature-induced dimensional changes of the constituents of advanced composites are summarized in the following sections.

1.1. Fibres

Both Kevlar aramid fibres and graphite fibres show highly anisotropic thermal expansion behaviour, with small shrinkage observed in the fibre direction as the temperature is increased. It is believed that the thermal expansion behaviour of both Kevlar and graphite fibres can be adequately described by two independent thermal expansivities parallel and perpendicular to the fibre axis. Representative values are shown in Table I [1].

1.2. Epoxy matrix resins

During the curing of epoxy resins, volume changes occur, which are associated with temperature changes and the progress of the chemical cross-linking reaction. In general the net volume change between the cured and the uncured state of the resin compared at ambient temperature is a reduction in volume (shrinkage) of 1 to 6%, depending on the type of resin, and the cure conditions. During some part of the cure cycle, however, the volume of the resin being cured may differ much

0022–2461/85 $03.00 + .12

TABLE I Thermal and mechanical properties of fibres and matrices

	Graphite	Kevlar	Polysulfone	BP907
α_L (ppm °C^{-1})	−0.36	−2	–	–
α_R (ppm °C^{-1})	18	59	–	–
E_L (GPa)	220	124	–	–
E (GPa)	–	–	2.48	3.10
α (ppm °C^{-1})($T < T_g$)	–	–	70	40
T_g (°C)	–	–	185	120
T_{cure} (°C)	–	–	–	177

more from the volume in the final cured form than might be indicated by the net comparison at room temperature of the cured and uncured resins. Work by Yates *et al.* [2] may be consulted for experimental techniques to study polymerization shrinkage, and for information on several specific systems.

Once cured, the thermal expansion behaviour of epoxies is comparable to that of other polymers. The thermal expansion coefficient decreases with decreasing temperature, and it is expected to reach zero as the zero point is reached on the absolute temperature scale. At transition points, such as the glass-transition point, or secondary transition points, there may be fairly sudden and significant changes in the thermal expansivity. Over relatively small temperature intervals (50 to 150° C, for example) the linear thermal expansivity can often be approximated by a temperature independent value of 40 to 80 ppm °C^{-1} [1, 2]. For a discussion of the temperature dependence of the thermal expansivity in several specific resin systems, work by Yates *et al.* [4] is available.

1.3. Thermoplastic matrix resins

Although thermoplastics have not been used in advanced composites in the past, their properties (toughness, and, in some cases, their excellent chemical stability) might recommend them for such use. The processing of thermoplastics in advanced composites can involve solutions of the polymer at some early stages of the process, but eventually it must involve the polymer melt. The soldification from the melt state (in which a polymer could reasonably be described as a highly viscous liquid, endowed with some elastic properties, especially on a short time scale) into a solid polymer is a purely physical process, involving the formatiom of a glass, or (partial) crystallization, or both, at characteristic temperatures. Themoplastics have to be cooled through these characteristic temperatures before they become form stable. The solidification process in thermoplastics is thermally reversible, in contrast to the irreversible chemical solidification of thermosetting resins, such as epoxies.

Over the last few years the volume changes associated with melting and solidification in thermoplastics have been investigated widely; e.g. [5–8]. Progress has also been made in understanding the role of pressure in these processes [5–8], and in understanding the equations of state of thermoplastic polymers in their various states (melt, glassy, crystalline) [8–15]. Generally, it can be said that the volume shrinkage (at atmosperhic pressure) of thermoplastics between their processing temperature and ambient temperature is at least 10% and can be as high as 30% (see below).

These shrinkages are, of course, very large, and they would make it very difficult to form precise parts of thermoplastics even in conventional injection moulding. In injection moulding, much smaller mould shrinkages are actually observed. This is achieved by the use of high pressures of 100 to 200 MPa, even 500 MPa in some cases. The volume shrinkage then is essentially the difference between the decreased specific volume of the melt at the injection pressure and the "normal" specific volume at ambient conditions. Such high moulding pressures also effect the transition temperatures by several tens of degrees (see below), and they influence the solidification process in this sense, also.

By contrast to the several hundred MPa pressure used in injection moulding, the processing of epoxy matrix composites generally involves pressure no higher than 0.5 to 1.5 MPa. In view of the very high viscosity of many thermoplastic melts, it seems possible that higher pressures than 1.5 MPa will be required for the processing of thermoplastic matrix composites. Just how high remains entirely open, but the inclusion of pressure in the following discussion will permit,

in each individual processing situation, to assess whether pressure can be expected to play a role in the solidification process.

In this paper, we begin by discussing the complex thermal expansion behaviour shown by thermoplastics. Then, the thermal stresses introduced during fabrication of thermoplastic or thermoset matrix composites are measured using photoelasticity. The build-up of these stresses correlates with the matrix thermal expansion behaviour.

2. Materials and methods

2.1. Thermal expansion behaviour of thermoplastics

The pressure dilatometer we use in our own work has been described in detail [6, 16]. In principle, the volume change of a sample together with a known amount of confining fluid (generally mercury) is determined as a function of temperature (to above 400° C) and pressure (to 200 MPa). The volume change of a sample is determined by subtracting out the known volume change of the confining fluid. Both isothermal and isobaric measurements can be made, and we will discuss results obtained in both modes of experimentation.

2.2. Photoelasticity measurements

The photoelastic measurements of the thermal stresses were performed on unidirectional composite tapes made by wrapping yarns of Union Carbide T300 graphite fibres around steel plates between film layers of the desired matrix. The assembly was then vacuum-bagged and pressed under conditions which depended on the matrix.

Union Carbide Polysulfone P-1700 was obtained in a 0.76 mm thick film from Westlake plastics. One sheet of film was used on each side of the graphite fibres. The tapes were pressed at 300° C with pressures between 0.34 and 3.4 MPa and times from 25 to 100 min. Well-impregnated samples were achieved with 1.0 MPa pressure for 25 min. From the composite tape density, we estimate the fibre volume fraction of the graphite/polysulfone composite tapes to be 33 ± 5%.

American Cyanamide BP907 epoxy was obtained in B stage film form at 0.106 kg m^{-2}. Two sheets of the film were used on each side of the graphite fibres. The tapes were cured at 0.34 MPa by heating at 6° C min^{-1} to 177° C (350° F), holding at 177° C for 1 h and cooling slowly under pressure to below 60° C. From the composite tape density, we estimate the fibre volume fraction of the graphite/BP907 composite tapes to be 35 ± 5%.

Experiments on the variation of intensity with angle were done by attaching an EG & G UV 444B photodiode to the eyepiece of a Nikon polarizing microscope. All optical retardation experiments were performed using a programmable Metter hot stage and a Zeiss polarizing microscope. The retardation was measured with an Eringhaus rotary compensator.

3. Typical expansion/shrinkage behaviour of thermoplastics

There are basically two types of thermal expansion/shrinkage behaviours observed in thermoplastics: that of glass-forming polymers and that of crystallizable polymers. As representative of the class of glass-forming polymers, we will discuss Polysulfone P-1700 (PSF) made by Union Carbide. In Fig. 1 we have plotted isobars, which actually represent crossplots of the original, isothermal data. At zero pressure, there is a break in the volume/temperature curve near 185° C, which represents the zero (atmospheric)-pressure glass-transition temperature of polysulfone. Similarly, one can define the higher pressure glass-transition temperatures by the intersection of the appropriate extrapolated (dashed) glassy isobars with the melt isobars, yielding line A in Fig. 1. Along this line we have $dT_g/dP = 0.58°\,C\,MPa^{-1}$, which is typical for the pressure dependence of the glass-transition temperature of amorphous thermoplastics. Between lines A and C (which is an isotherm through the zero-pressure glass-transition temperature) there is a peculiar dip in the isobars. This is a consequence of the isothermal mode of measurement in these experiments. New glasses with new properties are formed whenever a melt is vitrified by applying pressure, rather than by cooling. Among other things, such pressure-formed glasses are densified, i.e. they are denser than a glass formed at zero pressure would be at the same temperature and measuring pressure. This is fully discussed by Zoller, [17], and is just one example of how glass formation and glassy properties depend on the path taken in the formation of a glass. A better known example of this path dependence is the dependence of glassy properties on cooling rate, which has been discussed very extensively.

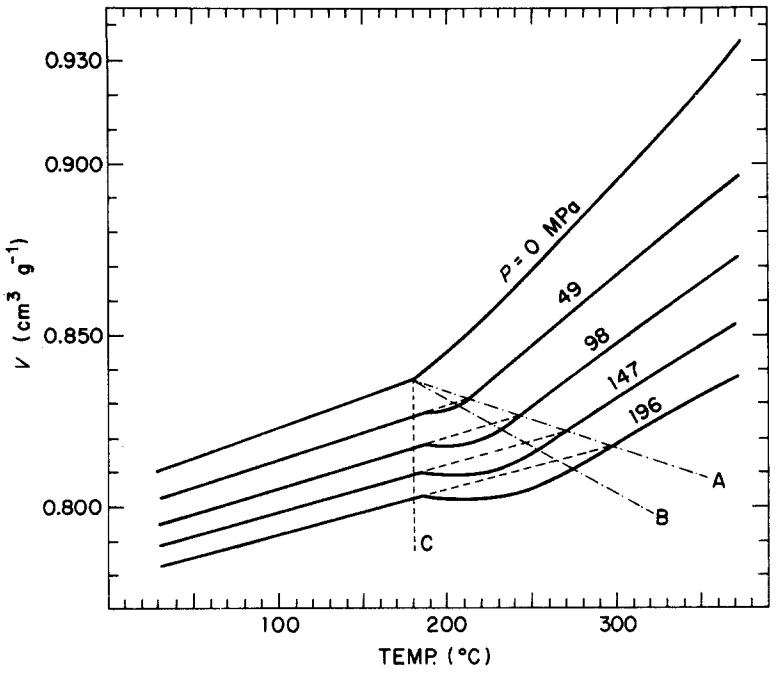

Figure 1 Specific volume of polysulfone as a function of temperature and pressure. Line C is an isotherm through the zero-pressure glass-transition temperature. Line A denotes the pressure-dependent glass-transition temperature of the original glassy material, line B the glass-transition line of pressure-formed glasses (see [17]).

Both for glasses and melts of thermoplastics, it is possible to describe the dependence of specific volume on temperature and pressure mathematically. We use the so-called Tait equation for the volume dependence on pressure along an isotherm:

$$V(P, T) = V(0, T)\{1 - 0.0894 \ln [1 + P/B(T)]\}, \quad (1)$$

in which the Tait parameter, $B(T)$ depends on temperature as follows

$$B(T) = B_0 \exp(-B_1 T). \quad (2)$$

Together with any suitable fit for the atmospheric pressure volume $V(0, T)$, the Tait equation can generally be fitted to represent the data of glasses (i.e. point to the left of the line C in Fig. 1) and melts (point to the right of line A in Fig. 1) to better than $0.002\,cm^3\,g^{-1}$ [11, 12]. In the transition region, i.e. between lines A and C, the fitting parameters for the glass will yield the extrapolation of the volume of the starting glass (i.e. the extrapolated, dashed lines in Fig. 1). For polysulfone we find:

glass: $V(0, T) = 0.8051 + 1.756 \times 10^{-4}\, T$

$$B(T) = 432 \exp(-1.543 \times 10^{-3}\, T)$$

melt: $V(0, T) = 0.7664 + 3.419 \times 10^{-4}\, T + 3.126 \times 10^{-7}\, T^2$

$$B(T) = 366 \exp(-3.757 \times 10^{-3}\, T)$$

(T in °C, P and B in MPa, V in $cm^3\,g^{-1}$).

It is generally agreed that the Tait equation is purely empirical. Its utility lies in the fact that it lends itself to a relatively simple calculation of the thermal expansivity $\alpha(P, T) = (d\ln V/dT)_P$ and of the isothermal compressibility $\kappa(P, T) = -(d \ln V/dP)_T$ as follows:

$$\alpha(P, T) = \alpha_0 - \kappa(P, T) P B_1, \quad (3)$$

in which α_0 is the thermal expansivity at zero pressure,

$$\kappa(P, T) = \{(P + B)[11.185 - \ln(1 + P/B(T))]\}^{-1}, \quad (4)$$

with $B(T)$ the Tait parameter as given in Equation 2 above.

Using these equations and the fitting parameters given for polysulfone, we calculate an atmospheric pressure thermal expansivity near $2.1 \times 10^{-4}\,°C^{-1}$ for all temperatures in the glass and about $5.9 \times 10^{-4}\,°C^{-1}$ for the melt at 300° C. The compressibility at zero pressure in the

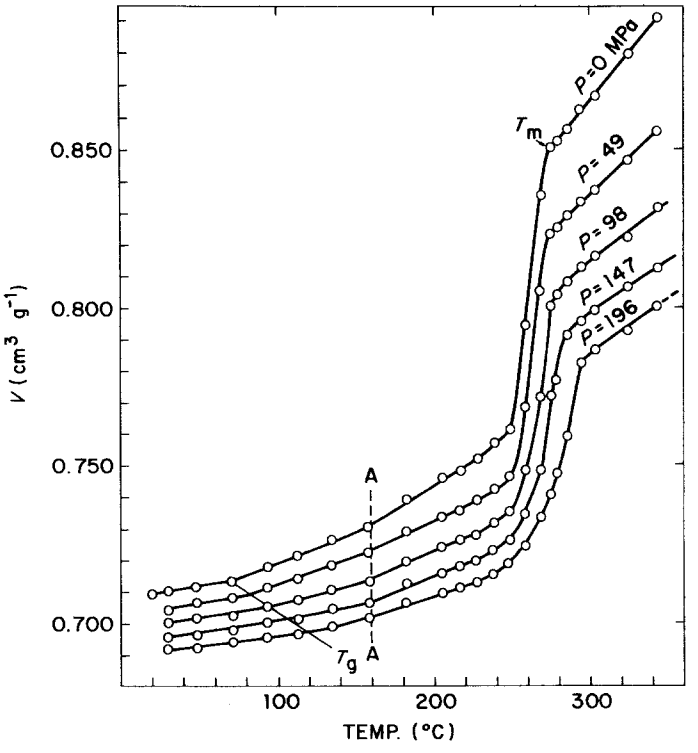

Figure 2 Specific volume of poly(ethylene terephthalate) as a function of temperature and pressure. T_m is the end of the melting interval at zero pressure. Line T_g and A denote the glass transition and a secondary transition, respectively (see [15]).

glass at 30° C is about 0.22×10^{-3} MPa^{-1} while it is about 0.75×10^{-3} MPa^{-1} in the melt at 300° C. Generally, both the expansivity and the compressibility are strongly temperature- and pressure-dependent, but at any pressure and temperature they can be calculated reliably given the above expressions. Tait equation fits are available for a number of other polymers as well.

A representative example of the dependence of the specific volume on temperature and pressure of a crystallizable polymer is given in Fig. 2 for poly(ethylene terephthalate) (PET) [18]. It is well known that polymers do not crystallize completely. To what extent they crystallize, and what the crystalline and amorphous morphologies are, depends on the path taken from the equilibrium melt state into the solid state. Cooling rates, stresses (e.g. pressures) and flow fields during solidification can, and do, affect solid structure and solid properties. Even in an already partially crystalline sample the overall level of crystallinity can often be increased, and the morphology can be altered by annealing treatments, preferably at temperatures between the glass-transition temperature and the melting point. Some polymers (e.g. polyethylene) crystallize so readily and rapidly that it is hard to affect the overall level of crystallinity of reasonably thick samples (1 mm or thicker). Others, and PET is among them, can be prevented from crystallizing by very fast cooling, and can be obtained in completely amorphous form. Because there can be differences of several per cent in the densities of the amorphous and crystalline form of the same polymer (e.g. for PET the amorphous density at 20° C is 1.335 g cm^{-3} [19], and the crystalline density is 1.45 to 1.49 g cm^{-3} [7]), it is necessary to specify the state of a partially crystalline material in plots such as those of Fig. 2.

The starting material for the data in Fig. 2 was a PET sample which has been annealed at 100° C for 12 h (mostly to reduce the moisture content), followed by an annealing of 0.5 h at 220° C to maximize the crystallinity. This sample had a density of 1.409 g cm^{-3}, which corresponds to a crystalline content around 50%, by interpolating between the crystal and amorphous densities quoted above. The intensity of the glass transition near 70° C (Fig. 2) is much reduced because of the crystallinity, and the most striking feature of the *PVT* relationship is the large volume change on melting. As a consequence of the volume expansion due to melting, the overall volume change at

atmospheric pressure between 300 and 30° C is 21% for PET, while it was about 10% for PSF. Some of that difference is due to crystallization/melting, but even amorphous PET with a room-temperature density of 1.335 g cm^{-3} would show a volume change of 15%, due, in part to its lower glass-transition temperature. With a lower T_g, a larger portion of the temperature change from 300 to 30° C is associated with the larger volume expansion coefficient that all polymers have above T_g.

The Tait equation can again be used to describe the compressibility behaviour of the melt with

$$B(\text{MPa}) = 369 \exp [-4.15 \times 10^{-3} T(^\circ \text{C})] . \quad (5)$$

However, the solid state data cannot be adequately fitted to the Tait equation. Derivatives for compressibility and thermal expansivity of the solid have to be obtained by direct differentiation. For comparison with PSF we quote the zero-pressure expansion coefficient of PET at 30° C (1.07×10^{-4} ° C^{-1}) and at 300° C (6.8×10^{-4} ° C^{-1}), and the zero-pressure compressibilities at 30° C (0.18×10^{-3} MPa^{-1}) and 300° C (0.84×10^{-3} MPa^{-1}). In the melt both derivative parameters are somewhat larger for PET than for PSF, in solid state they are somewhat smaller because of crystallinity. Nevertheless, these values are relatively large compared to other types of materials, such as metals, or inorganic glasses, but they are typical of thermoplastics as a class of materials.

The melting point is defined as the end of the melting interval (marked as T_m on the zero-pressure curve in Fig. 2). The corresponding points on the higher pressure isobars do not represent the pressure dependence of the melting point, because the lines represent isobaric crossplots of isothermal data. If a melt is compressed isothermally, starting from $P = 0$, the question of whether crystallization will occur or not is not just a question of thermodynamics (i.e. the question whether the pressure exceeds the melting pressure for that particular temperature), but also a question of kinetics (whether crystals will actually form during the duration of the experiment). It is well kown that polymer melts supercool readily, i.e. they will crystallize at lower temperatures (or higher pressures) than they melt [5]. This is shown in Fig. 3, in which data from an isobaric run are plotted. A previously

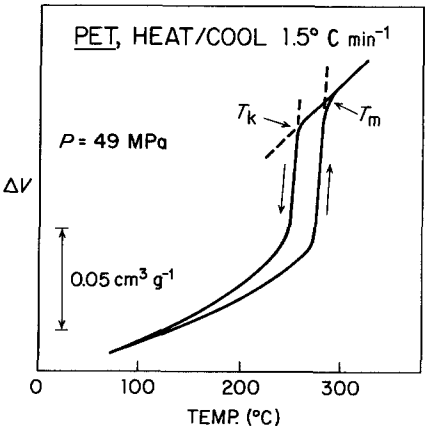

Figure 3 Isobaric heating and cooling experiment on poly(ethylene terephthalate) showing the melting and crystallization transition.

annealed sample of PET was heated at 1.5° C min^{-1} at a constant pressure of 49 MPa, starting from room temperature. The end of the melting interval (T_m) was found at about 285° C. At 310° C the cooling cycle was started at the same rate. Crystallization started at $T_K = 258^\circ$ C, i.e. with a supercooling of about 27° C with respect to the melting point at the same pressure. In Fig. 4 we have plotted the results of several runs of this type. Both T_m and T_K increase with pressure by about 0.47° C MPa^{-1}; i.e. the supercooling is virtually independent of pressure. The cooling rate, however, has a profound influence on supercooling: increasing the cooling rate increases the supercooling.

We went through this discussion of the *PVT* behaviour of typical thermoplastics to demonstrate the complexity of behaviour that can be expected during the solidification step in the manufacturing of thermoplastic matrix composites.

4. The solidification shrinkage of several thermoplastics

In Fig. 5 we have plotted the zero (atmospheric) pressure volume expansion of several thermoplastics, expressed as a percentage change with respect to the volume at 30° C. Indicated on each curve are suggested processing temperatures for these materials. All data are from our own measurements, with the exception of the epoxy, where we used a volume expansion coefficient of 120×10^{-6} ° C^{-1} for a typical 177° C (350° F) cure material (e.g. Hercules 3501-6 resin [3]). The volume changes between ambient temperature

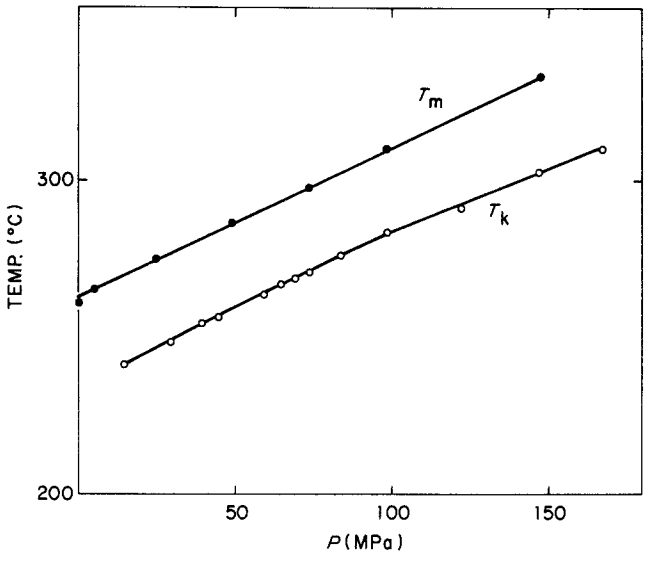

Figure 4 Pressure dependence of the melting (T_m) and crystallization (T_k) temperatures of poly(ethylene terephthalate). The two lines are essentially parallel, indicating supercooling independent of pressure.

and processing temperature are listed in Table II. It is quite clear that the crystallizable polymers – polyethylene (PE), polypropylene (PP), and poly(ethylene terephthalate) (PET) – show a considerably larger volume change than the amorphous polymers – polycarbonate (PC), polysulfone (PSF) and poly(methylmethacrylate) (PMMA). From their processing temperatures to ambient temperature, all thermoplastics have volume changes several times that of the epoxy shown. We will discuss below the build-up of stresses in a composite that is caused by the volume change in the matrix, which is not matched by the fibres. Naturally, a melt of a thermoplastic is not able to support non-hydrostatic stresses for any length of time; it flows to relieve the stress. In order to judge a matrix material with respect to the potential for stress build-up due to unmatched volume changes in the matrix, the volume shrinkage below the temperature where the matrix has assumed enough of a solid-like character to support stresses, should be considered relevant. A thermoplastic reaches an effectively solid-like character at the glass transition temperature if it forms a glass, and probably somewhere into the crystallization range if it can form crystals. These temperatures are indicated by circles in Fig. 3, and the corresponding volume changes are listed in Table II. Judged in this way, glass-forming thermoplastics have about the same volume changes as the typical 177° C cure epoxy, but the crystallizable materials have the potential of much higher shrinkage.

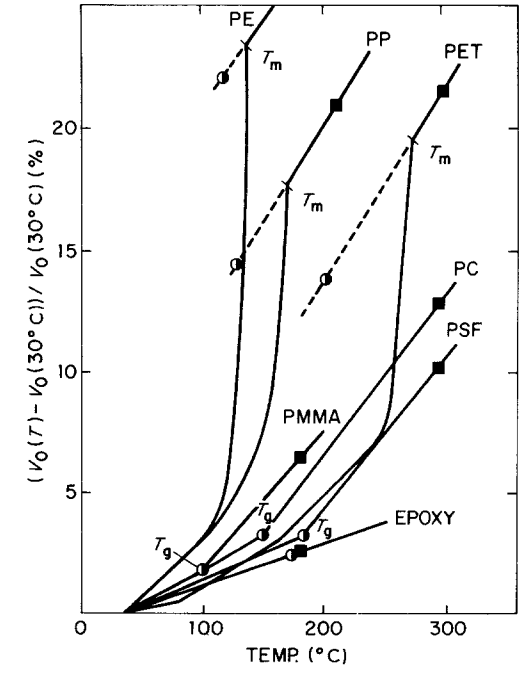

Figure 5 Zero-pressure volume expansion (relative to volume at 30° C) of several thermoplastics. Squares designate typical processing temperatures, circles the onset of solidification (crystallization or glass formation) at slow cooling rate (1 to 2° C min^{-1}).

5. Photoelastic measurement of the thermal stresses in composites

The unidirectional composite tapes used for measuring the thermal stresses had fibre volume fractions in the range of 30% to 40%. This is the highest volume fraction we can achieve and still be able to find areas between fibres for optical

TABLE II Volume and linear dimensional changes during composite processing of several thermoplastics and a typical epoxy between the indicated temperature and 30° C

	From processing temperatures			From solidification temperatures		
	T (° C)	$\Delta V/V_0$ (%)	$\Delta l/l_0$ (%)	T (° C)	$\Delta V/V_0$ (%)	$\Delta l/l_0$ (%)
Polyethylene	195	29	8.9	120	22	6.8
Polypropylene	215	22.5	7.0	125	14.2	4.5
Poly(ethyleneterephthalate)	290	21	6.6	200	13.6	4.3
Polycarbonate	295	12.7	4.1	160	3.2	1.0
Polysulfone	295	10.3	3.3	185	3.2	1.0
Poly(methyl methacrylate)	180	6.5	2.1	102	1.9	0.6
Epoxy	177	2.5	0.7	177	2.5	0.7

observation of the matrix. Although our composite tapes have lower fibre volume fractions than commercial composites, which are typically 50% to 60%, they are still useful as a model system. In particular, these tapes are a good model system for studying stresses in the fibre direction. The reason is that the longitudinal modulus of the graphite fibres ($E_L = 220$ GPa) is much greater than the moduli of the matrices ($E = 2.48$ GPa for PSF and 3.10 GPa for BP907) and, therefore, the fibres dominate the longitudinal composite properties. As shown in the discussion, the longitudinal thermal stresses in our model composite are expected to be only slightly lower than the longitudinal thermal stresses in commercial unidirectional composites.

The residual stresses in the matrix were examined using the photoelastic effect. We began by observing the isoclinic fringes. To study these fringes, we focus on a portion of the matrix between fibre yarns while the sample is between crossed polarizers. As the sample is rotated with respect to the crossed polarizers, we expect to see fringes when the principal stress direction aligns with the crossed polarizer [19]. We find that the entire 100 to 200 μm wide matrix region used for observation forms a fringe at the same angle indicating a unique principal stress direction. In Fig. 6, we determine the principal stress direction by plotting the relative intensity of transmitted light against angle between the crossed polarizers and the fibre direction. As expected,

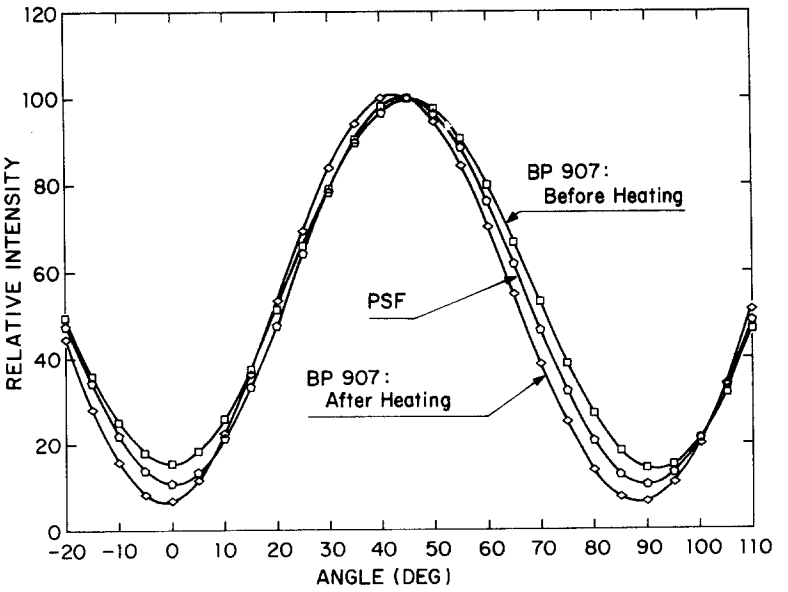

Figure 6 Relative intensity of transmitted light through the matrix of composite tapes placed between crossed polarizers as a function of the angle between the fibre direction and the orientation of the cross polarizers. The minimum intensity indicates the presence of an isoclinic fringe.

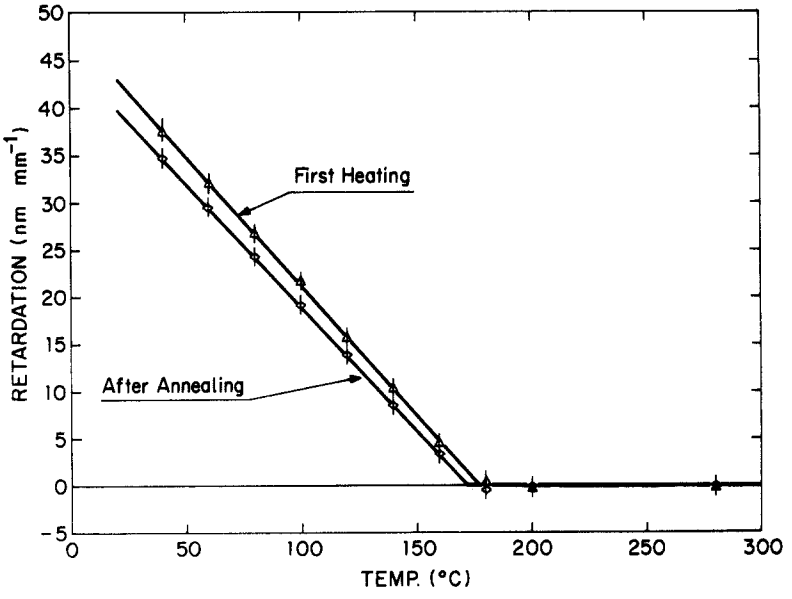

Figure 7 Optical retardation per mil of thickness as a function of temperature for graphite/PSF composite tapes. "After annealing" curve obtained from composite tapes annealed 100° C above T_g for 5 min before the measurement.

the maximum extinctions are at 0 and 90°, that is, the principal stress directions are parallel and perpendicular to the fibre direction.

The magnitude of the thermal stresses can also be estimated by the photoelastic effect. The average of the difference between the principal stresses in the plane of the model composite is given by [20]:

$$\langle \sigma_{\parallel} - \sigma_{\perp} \rangle = \frac{R}{Cd}, \tag{6}$$

where R is the optical retardation in nm, C is the photoelastic sensitivity of the matrix in Brewsters, d is the sample thickness in mm, and the principal stresses are in MPa. The average of $\sigma_{\parallel} - \sigma_{\perp}$ is over the region of observation and through the sample thickness.

Fig. 7 is a plot of the optical retardation per mil against temperature for graphite/PSF composite tapes. The curve for the first heating is an average of five samples made under different conditions. All five were pressed at 300° C but the amount of time and pressure was varied. In the two extremes we achieved samples with poorly impregnated yarns and samples with well-impregnated yarns. Despite the various conditions, the spread of the data is very small. Table III lists the optical retardation per mil of the five samples at 30° C and the standard deviation of the measurements. The experimental uncertainty in each R/d value is ± 1 nm mil^{-1} (1 nm mil^{-1} = 39.4 nm mm^{-1}).

As discussed above, the T_g for PSF is 185° C [17]; above T_g the optical retardation is zero. In other words, the optical retardation per mil is well described by the truncated function

$$R/d = k(T_0 - T)_+, \tag{7}$$

where T is the temperature, T_0 is the reference stress free state, and k is a constant. The results of a fit to this equation are given in Table IV. Two important points are: (1) T_0 of 177° C is close to the T_g for PSF; and (2) R/d at 25° C is

TABLE III Thermal stress measurement results for five samples of graphite/PSF at 40° C. The errors in the averages are standard deviations of the five samples

Sample	R/d (nm mil^{-1})	$\langle \sigma_{\parallel} - \sigma_{\perp} \rangle$
1	36.6	4000
2	37.5	4100
3	38.3	4188
4	37.4	4090
5	37.7	4122
Average	37.5 ± 0.6	4100 ± 70

TABLE IV Results of a fit of the R/d for graphite/PSF composites to Equation 7

	First heating	After annealing
k	0.274	0.262
T_0 (° C)	177	172

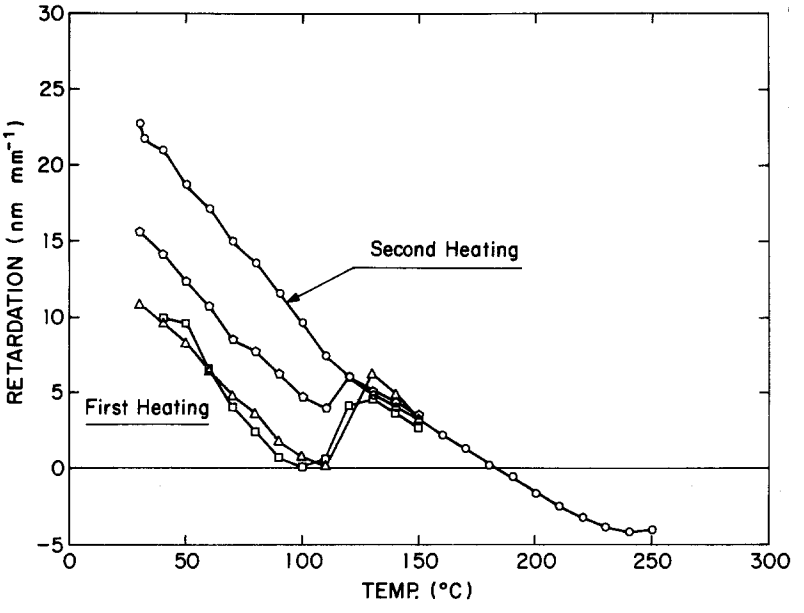

Figure 8 Optical retardation per mil of thickness as a function of temperature for graphite/BP907 composite tapes. The first heating curves are for three samples that had not been heated since the curing step. The second heating curves is an average of the same three samples after they had been heated once to 150° C.

41.6 ± 1 nm mil^{-1}. From this R/d and the photoelastic sensitivity of PSF which we measured to be 52.5 ± 3 Brewsters, we find that $\langle \sigma_{\parallel} - \sigma_{\perp} \rangle =$ 31.4 ± 2 MPa at 25° C. This stress level is very high and is above the Union Carbide specifications for use of PSF in water environments [21].

The second curve in Fig. 2 is from four samples annealed 100° C above T_g for 5 min before the measurement. As shown in Table II, there is less than a 5% change in the two fitting parameters. We conclude, as expected, that the thermal stresses in this constrained system cannot be significantly affected by annealing.

Fig. 8 shows a plot of the optical retardation per mil against temperature for graphite/BP907 composite tapes. The three lower curves are data for the first heatings of three different samples. All the curves decrease monotonically until 110 to 120° C, at which point there is a jump up to the curve for the second heating. After cooling, all R/d against temperature curves fall near the second heating curve which is an average of the three samples. The point 110 to 120° C is identical to the T_g as measured by DSC for this epoxy system. We conclude that the as-cured composite tape which is cured and cooled under pressure has frozen in nonuniform stresses and in the locations we examine between the fibres, the average stress is lower than the average stress over the whole sample. After heating above T_g, the stresses become more uniform. In support of this conclusion, we find more complete extinction of transmitted light through the matrix after one heating above T_g. This effect, which is seen in the two BP907 curves of Fig. 6, indicates more uniform principal stress directions in the sample heated only once.

For a characterization of thermal stress build-up, we look at the curve for the second heating. From that curve and the photoelastic sensitivity of BP907 which we measure to be 46.0 ± 3 Brewsters, we find that $\langle \sigma_{\parallel} - \sigma_{\perp} \rangle = 20.0 \pm 2$ MPa at 25° C. Unlike the amorphous thermoplastic PSF, the R/d curve does not drop to zero at T_g but only changes in slope. The results of fits of the data to $R/d = k\,(T_0 - T)$ above and below T_g are given in Table V. From the fit, R/d drops to zero at 184° C which is close to the cure temperature of 177° C (350° F. After dropping to zero, however, the stresses do not remain at zero at higher temperatures: the dominant stress

TABLE V Results of a fit to $R/d = k'(T_0 - T)$ for the linear region of graphite/BP907 composite tapes

Temperature range	k'	T_0
30 to 100	0.183	153
140 to 200	0.093	184

along the fibre direction changes from tensile to compressive. This change causes the fast and slow axes of the birefringent matrix to be interchanged from their positions below T_c. The result is that the Ehringhaus compensator changes from the subtractive to the additive position and we measure a negative optical retardation.

6. Discussion of the thermal stress measurement

There is a significant mismatch between the thermal expansion properties of graphite fibres and the two matrices involved in this study. A list of the thermal expansion coefficients for graphite and for the two matrices below their T_gs is given in Table I. The thermal property mismatch in the transverse direction is smaller than in the longitudinal direction. For a first approximation, we will assume the transverse stresses are small compared to the longitudinal stresses. The resulting one-dimensional linear elastic stress analysis can be solved to give

$$\sigma_{\parallel} = \int_{T}^{T_0} \frac{\Delta\alpha E_m E_L V_f}{E_m V_m + E_L V_f} dT, \qquad (8)$$

where $\Delta\alpha$ is the difference between the longitudinal thermal expansion coefficient of the fibre and the thermal expansion coefficient of the matrix, T is the temperature, T_0 is the temperature for the onset of stress build-up, E_L and E_m are the longitudinal Young's modulus of the fibre and the Young's modulus of the matrix, and V_f and V_m are the volume fractions. All the properties may depend on temperature, but if they are temperature independent in the range of stress build-up, we have

$$\sigma_{\parallel} = \frac{\Delta\alpha E_m E_L V_f}{E_m V_m + E_L V_f} (T_0 - T). \qquad (9)$$

For graphite and Kevlar aramid fibres, $E_L \gg E_m$ and $E_L V_f/(E_m V_m + E_L V_f)$ quickly approaches 1 as V_f increases. Therefore, above $V_f = 10\%$, $\sigma_{\parallel}$ is nearly independent of V_f. For this reason the stresses we measure of composite tapes with $V_f = 30\%$ to 40% are of comparable magnitude to unidirectional composites with commercial fibre volume fractions of 50% to 60%.

Because the transverse stresses probably cannot be ignored, we have examined their magnitude by solving the three-dimensional stress problem for a composite cylinder model. The composite cylinder model is an anisotropic fibre surrounded by a cylinder of an isotropic matrix. The results [22] show that Equations 8 or 9 are very accurate when $\Delta V_{matrix} = \Delta V_{fibre}$ where ΔV is the total volume change on cooling. At this point the transverse stresses are near zero and a one-dimensional constrained shrinkage analysis is appropriate. For both matrices used, however, $\Delta V_{matrix} > \Delta V_{fibre}$. In this case, the three-dimensional stress analysis predicts that equation 9 is a lower bound for the longitudinal stress.

Adopting Equation 9 as a lower bound to $\sigma_{\parallel}$, we can place bounds on the transverse stresses for graphite/PSF and graphite/BP907 composite tapes. From Fig. 6, we see that for graphite/PSF composite tapes, $\langle\sigma_{\parallel} - \sigma_{\perp}\rangle$ is proportional to $(T_0 - T)$ below 177° C. If we make the assumption that $\sigma_{\parallel}/\sigma_{\perp}$ is fairly constant with temperature, then $\sigma_{\parallel}$ is also proportional to $(T_0 - T)$. This fact means that the mechanical properties in Equation 9 are independent of temperature below 177° C. Using the properties in Table I and $V_f = 0.33$, we find

$$\langle\sigma_{\parallel}\rangle \gtrsim 25.7\,\text{MPa} \qquad (10)$$

at 25° C. From the measured value for $\langle\sigma_{\parallel} - \sigma_{\perp}\rangle$, we can estimate that the average transverse stresses are

$$\langle\sigma_{\parallel}\rangle \gtrsim -5.7\,\text{MPa}. \qquad (11)$$

We see that the matrix is in compression transverse to the fibre direction.

The R/d curve for graphite/BP907 is not linear over its entire range. In the portion of the curve below T_g (30° C to 100° C), however, it is linear. Using T_0 in Table III from a fit to this portion of the curve and the proportionality constant for Equation 9 derived from the properties in Table IV, we find with $V_f = 0.35$ that

$$\langle\sigma_{\parallel}\rangle \gtrsim 15.2\,\text{MPa} \qquad (12)$$

at 25° C. This value translates to a compressive stress in the transverse direction of

$$\langle\sigma_{\perp}\rangle \gtrsim -4.8\,\text{MPa}. \qquad (13)$$

Equation 8 is useful for describing features of the plots of optical retardation against temperature plots. First, we rewrite Equation 8 for the case of high modulus fibres such as graphite of Kevlar 49 aramid fibres. For these fibres $E_L \gg E_m$ and

$$\frac{E_L V_f}{E_L V_f + E_m V_m} \approx 1. \qquad (14)$$

This relation holds over the temperature ranges

we are using. Equation 8 becomes

$$\sigma_{\parallel} \gtrsim \int_{T}^{T_0} \Delta\alpha E_m \, dT \qquad (15)$$

which implies that the slope of optical retardation against temperature is proportional to $\Delta\alpha E_m$.

When an amorphous thermoplastic is heated above its glass transition the thermal expansion coefficient increases and the modulus decreases. The thermal expansion coefficient increase, however, is usually small when compared to the modulus decrease which can be several orders of magnitude [23]. This fact agrees with our observations. At T_g, the slope drops dramatically; within the accuracy of our measurements the slope drops to zero. In contrast, the modulus of highly cross-linked systems such as epoxies will not show a dramatic decrease at T_g [23]. At T_g for BP907 we see a slight decrease in the slope of the optical retardation plot. This decrease indicates that the modulus of BP907 drops more than the thermal expansion coefficient increases.

An important class of matrix candidates on which we have not performed photoelastic experiments, are semicrystalline thermoplastics. Typically, the modulus of semicrystalline thermoplastics does not drop as dramatically at T_g as it does for amorphous thermoplastics [23]. We, therefore, expect that the stresses will not drop to zero near the glass transition but instead at some higher temperature such as the melting point. As pointed out above, crystallization of thermoplastics is often marked by large volume changes. For analysis by Equation 8, these large volume changes are effectively large thermal expansion coefficients during crystallization. Thermal stress build-up from a high melting point through a crystallization transition could result in very high residual stress levels.

7. Conclusions

The large thermal property mismatch between graphite or Kevlar 49 aramid fibres and typical matrices can lead to large residual stresses. The expected tension in the matrix along the fibre direction can be estimated with a simple formula which involves the temperature-dependent expansion and mechanical properties of the matrix and the fibres. The complex thermal behaviour of many thermoplastics has been studied. It should be emphasized that the relevant experiments for use with composite matrices are the low-pressure volume-change experiments. These data are not equivalent to mould shrinkage data; in general thermoplastic shrinkage at low pressures is larger than the mould shrinkage. When using the correct shrinkage data, the measured residual stresses are in agreement with the calculated stresses.

The mechanism of stress build-up depends on the type of matrix. The analysis for epoxies or amorphous thermoplastics matrices is straightforward. In epoxies the stresses build up from the cure temperature. As pointed out by Hahn [24], however, the residual stress-free temperature may be lower than the cure temperature depending on the curing process. In amorphous thermoplastics the stresses build up from the glass-transition temperature. This fact is likely to be insensitive to typical processing conditions.

The mechanism of stress build up with semicrystalline thermoplastic matrices which has not been investigated may be complex and dependent on processing conditions. If the semicrystalline matrix assumes enough solid-like character early in the crystallization region, the constrained shrinkage will be large resulting in large residual stresses or cracking. If stress does not build up until after the crystallization is nearly complete, the stresses will be smaller but dimensional changes may be significant.

An important question is what effect the residual stresses will have on the composite properties. We expect that any composite property which depends on a matrix property that is affected by stress will be affected. Such properties include solvent sensitivity, impact toughness, fatigue, and compression. If the effects are large, it will be important to learn how to minimize the residual stresses. The most direct approach is to choose a matrix where stress build up is from a low temperature; i.e. to choose a matrix with a low T_g or cure temperature. This tactic is clearly limited by high-temperature property requirements of the composite. If a matrix has a high temperature for stress build-up, it may be possible to lower the stress-free temperatures by using a low T_g resin at the interface. When it is possible to vary the thermal properties of the matrix, the residual stress problem can be minimized by choosing a matrix with a total volume change on cooling from the stress build-up temperature which is approximately equal to, but slightly greater than, the corresponding volume change in the fibres. From an analysis of the composite cylinder model [22] we find that such a matrix

will have the minimum stress along the fibre direction under the restriction that the radial stress at the interface is still compressive. The volume change matching corresponds to a matrix whose average thermal expansion coefficient below the stress build-up temperature is 40 ppm $^{\circ}C^{-1}$ for a composite with Kevlar 49 aramid fibres and 12 ppm $^{\circ}C^{-1}$ for a composite with graphite fibres.

References

1. G. LUBIN, ED., "Handbook of Composites" (Van Nostrand Reinhold, New York, 1982).
2. B. YATES, B. A. McCALLA, L. N. PHILLIPS, D. M. KINGSTON-LEE and K. F. ROGERS, *J. Mater. Sci.* **14** (1979) 1207.
3. J. M. MAHISHI and D. F. ADAMS, *ibid.* **18** (1983) 447.
4. B. YATES, B. A. McCALLA, J. P. SARGENT, K. F. ROGERS, L. N. PHILLIPS and D. M. KINGSTON-LEE, *ibid.* **13** (1978) 2217.
5. B. WUNDERLICH, "Macromolecular Physics", Vol. 3, "Crystal Melting" (Academic Press, New York, 1980).
6. P. ZOLLER, Proceedings of the Eleventh North American Thermal Analysis Society, Vol. II (1981).
7. H. W. STARKWEATHER, P. ZOLLER and G. A. JONES, *J. Polymer Sci. Polymer Phys. Ed.* **21** (1983) 295.
8. P. ZOLLER, *ibid.* **20** (1982) 1453.
9. R. SIMHA and T. SOMCYNSKY, *Macromol.* **2** (1969) 342.
10. R. SIMHA, *ibid.* **10** (1977) 1025.
11. P. ZOLLER, *J. Polymer Sci. Polymer Phys. Ed.* **18** (1980) 157.
12. *Idem, ibid.* **18** (1980) 897.
13. R. K. JAIN and R. SIMHA, *ibid.* **17** (1979) 1929.
14. A. QUACH and R. SIMHA, *J. Phys. Chem.* **76** (1972) 416.
15. P. ZOLLER and H. H. HOEHN, *J. Polymer Sci. Polymer Phys. Ed.* **20** (1982) 2385.
16. P. ZOLLER, R. BOLLI, V. PAHUD and H. ACKERMANN, *Rev. Sci. Instrum.* **47** (1976) 948.
17. P. ZOLLER, *J. Polymer Sci. Polymer Phys. Ed.* **16** (1978) 1261.
18. P. ZOLLER and P. BOLLI, *J. Macromol. Sci. Phys.* **B18** (1980) 555.
19. J. BRANDRUP and E. H. IMMERGUT, EDS., "Polymer Handbook" (Interscience, New York, 1967).
20. A. W. HANDRY, "Photoelastic Analysis" (Pergamon Press, New York, 1966).
21. UDEL Polysulfone Product Data, Union Carbide (1981).
22. J. A. NAIRN, *Polymer Composites*, in press.
23. J. D. FERRY, "Viscoelastic Properties of Polymers" (Wiley, New York, 1970).
24. H. T. HAHN, *J. Comp. Mater.* **10** (1976) 266.

Received 30 December 1983
and accepted 10 April 1984